User-Side RIS: Realizing Large-Scale Array at User Side

Kunzan Liu, Zijian Zhang, and Linglong Dai

Beijing National Research Center for Information Science and Technology (BNRist)
Department of Electronic Engineering, Tsinghua University, Beijing 100084, China
Emails: lkz18@mails.tsinghua.edu.cn, zhangzj20@mails.tsinghua.edu.cn, daill@tsinghua.edu.cn

GLOBECOM 2021 - 2021 IEEE Global Communications Conference | 978-1-7281-8104-2/21/$31.00 ©2021 IEEE | DOI: 10.1109/GLOBECOM46510.2021.9685418

***Abstract*—Massive multiple-input multiple-output (MIMO) with a large-scale antenna array at the base station (BS) side is one of the most essential techniques for 5G wireless communications. However, due to the forbidden hardware cost and mismatched size, it is physically limited to deploy massive MIMO at the user side. To break this limitation, inspired by the promising technique called reconfigurable intelligent surface (RIS), we firstly propose the concept of user-side RIS (US-RIS) which is a cost- and energy-efficient realization for large-scale array at the user side. Different from the existing RISs that work as base-station-side RISs (BSS-RISs), US-RIS is the first usage of RIS at the user side. Then, we propose a novel architecture of user with the aid of US-RIS with a multi-layer structure for compact implementation. Based on the proposed multi-layer US-RIS, we formulate the signal-to-noise ratio (SNR) maximization problem in the US-RIS-aided communications. To tackle the challenge of solving this non-convex problem, we propose a multi-layer precoding design that can obtain the optimal parameters at transceivers and US-RIS by iterative optimization. Finally, simulation results are shown to verify the practicability and superiorities of the proposed multi-layer US-RIS as a realization of the large-scale array at the user side.**

***Index Terms*—Reconfigurable intelligent surface (RIS), multiple-input multiple-output (MIMO), multi-layer structure, joint precoding.**

I. Introduction

Massive multiple-input multiple-output (MIMO), which employs hundreds of antennas at the base station (BS) side, is one of the most essential technologies for 5G wireless communications [1]. By simultaneously serving massive users with precoding and combining operations, orders of magnitude increase in the sum spectral efficiency can be achieved by massive MIMO [2]. For typical users such as customer premises equipment (CPE), the deployment of a large-scale antenna array is also beneficial, because the large-scale array can enlarge the wireless coverage and form high gain beams to reduce the power consumption of the user. However, considering the forbidding cost and the mismatch of the large-scale array and user in physical size, the implementation of a large-scale array at the user side is usually considered as impossible.

Fortunately, a novel technique called reconfigurable intelligent surface (RIS) is recently proposed, which provides a possible solution to the realization of the large-scale array at the user side. Specifically, RIS is an array composed of numerous low-cost passive elements. By properly controlling the phase shift of each element, RIS can reflect or penetrate the incident electromagnetic wave to any desired direction with high array gains [3]–[5]. Due to its cost- and power-efficient characteristics, RIS is regarded as a revolutionary technique for future wireless communications [6]–[8].

Current usages of RIS can be generally divided into two categories. The first category is to employ relay-like RIS between the BS and the user to enhance transmission links. For instance, RIS can be utilized to enhance communications by overcoming blockage [3]. To increase the network capacity, RIS-aided cell-free network is proposed in [9]. In [10], RIS embodies its advantages by saving the transmit power of BS when serving users. The second category is to employ RIS at the BS side to realize beamforming with low cost and power consumption. One typical work proposes a RIS-based precoding architecture that replaces the phased array with RIS [11]. Other works like [12] provide designs that also utilize RIS at the BS side to realize beamforming with low cost and power consumption. To summarize, both two categories utilize RIS to improve the overall channel capacity of the cellular network, and thus we name them as base-station-side RISs (BSS-RISs). However, RIS has never been considered to be employed at the user side to our best knowledge.

In this paper, we propose the concept of user-side RIS (US-RIS) that enables the deployment of a large-scale array at the user side, which is also the first usage of RIS at the user side. Different from the existing BSS-RISs, US-RIS is designed for its centric user and can be regarded as a component of the user. Moreover, we propose a new architecture with the aid of US-RIS with a multi-layer structure for compact implementation. Furthermore, we formulate the signal-to-noise ratio (SNR) maximization problem in the US-RIS-aided communications. Due to the non-convexity of this optimization problem, we further propose a multi-layer precoding design that can obtain the optimal parameters at transceivers and US-RIS by iterative optimization. Finally, simulation results are presented to verify the practicability and superiorities of the proposed realization of the large-scale array at the user side[1].

Notation: $(\cdot)^{-1}, (\cdot)^*, (\cdot)^T$ and $(\cdot)^H$ denote the inverse, conjugate, transpose and conjugate transpose of a matrix, respectively; $[L]$ denotes the set of integers $\{1, 2, \cdots, L\}$; $\langle \boldsymbol{x} \rangle$ denotes the normalized vector of $\boldsymbol{x}$, i.e., $\langle \boldsymbol{x} \rangle = \boldsymbol{x}/\|\boldsymbol{x}\|_2$; $\arg(\cdot)$ denotes the phase angle for each element of a complex vector;

[1]Simulation codes are provided to reproduce the results in this paper: http://oa.ee.tsinghua.edu.cn/dailinglong/publications/publications.html.

978-1-7281-8104-2/21/$31.00 ©2021 IEEE

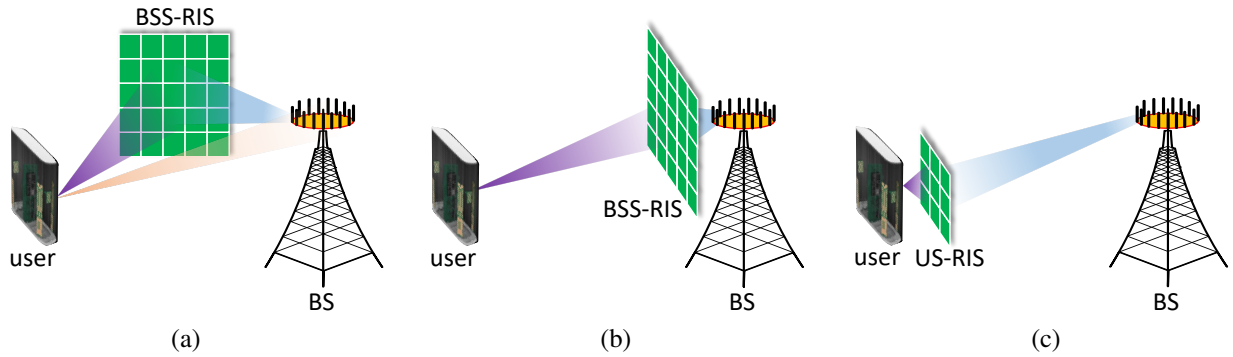

Fig. 1. Different communication systems utilizing RIS. (a) BSS-RIS-aided communications where relay-like RIS is employed between the BS and the user. (b) BSS-RIS-aided communications where RIS is employed at the BS side. (c) US-RIS-aided communications where RIS is employed at the user side.

diag$(\cdot)$ denotes the diagonal operation; $\psi_{\max}(\cdot)$ denotes the eigenvector of a matrix corresponding to its largest eigenvalue.

II. System Model

To realize a large-scale array at the user side with low cost, in this section, we propose the concept of US-RIS. Then, we propose a novel user architecture with a multi-layer US-RIS and develop the system model in US-RIS-aided communications.

A. Concept of US-RIS

As its name suggests, US-RIS is a hardware technique of integrating RIS at the user side, which aims to tackle the issue of forbidding cost to deploy large-scale array at the user side.

Traditional usages of RIS in wireless communications mainly consist of employing relay-like RIS between the BS and the user and employing RIS at the BS side, as shown in Fig. 1 (a) and (b), respectively. Specifically, in Fig. 1 (a), a relay-like RIS is used to reconfigure the wireless channels, while in Fig. 1 (b), RIS is deployed at the BS side to enable the BS beamforming. Since both of these two usages are aiming at improving the overall channel capacity of the cellular network, we would like to name them as BSS-RISs. While, in this paper, we focus on a novel usage of RIS, named US-RIS, as shown in Fig. 1 (c). Different from existing BSS-RISs, US-RIS is employed as a component of the user and serves as a large-scale array, which breaks the fundamental physical limit that a user can hardly own a large-scale array due to the high cost and the mismatch in size.

B. Architecture

To illustrate the applicability of the user architecture equipped with US-RIS, here we take a typical user as an example. Specifically, Fig. 2 (a) presents a real-world CPE with a size of $25\,\text{cm} \times 15\,\text{cm} \times 45\,\text{cm}$, while Fig. 2 (b) shows a user architecture equipped with US-RIS in perspective view. In Fig. 2 (b), three transmissive RISs are vertically stacked as a multi-layer structure, with a 2 cm gap between the adjacent layers. The overall size of the new CPE then becomes $25\,\text{cm} \times 21\,\text{cm} \times 45\,\text{cm}$ which is acceptable for domestic. Note that, for practical applications, the number of the RIS layers

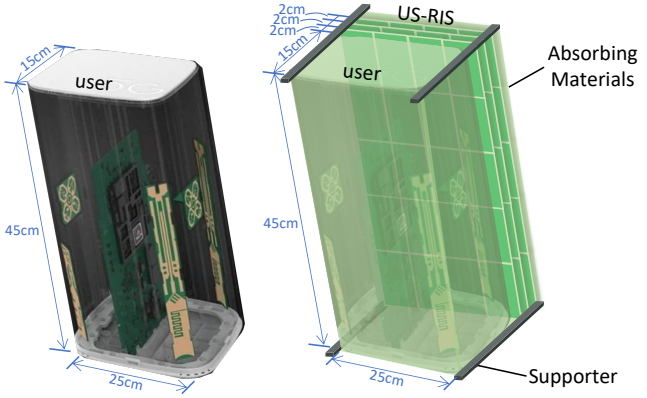

Fig. 2. Illustration of user architecture. (a) A real-world CPE. (b) The proposed user architecture equipped with a multi-layer US-RIS.

TABLE I
Comparison between BSS-RIS and US-RIS

Aspect	BSS-RIS	US-RIS
Location	BS	user
Controller	one/multiple BS(s)	one user
Beneficiary	one/multiple user(s)	one user
Operating mode	mainly reflective	transmissive
Structure	single-layer	single/multi-layer
Size	large	compact
EAR	small	big

and the inter-layer gaps are flexible, which depends on the specific user size. Besides, the configures of RIS elements are all controlled by the centric user, and the whole structure should be enclosed by supporter and absorbing materials to protect the stability of the internal channels from external interference.

To clarify the characteristics of this novel user architecture and the differences from existing BSS-RISs, here we summarize the key features of BSS-RIS and US-RIS in Table I and discuss their comparisons as follows.

- *Location, controller, and beneficiary:* According to their terminologies, the most essential difference between BSS-RIS and US-RIS is their location. The BSS-RIS is primarily proposed for improving the overall channel

capacity of the cellular network, while US-RIS at the user side is transmissive and may also be regarded as an integral component of the user. Hence, both the controller and the beneficiary of the BSS-RIS and US-RIS are different. The BSS-RIS is controlled by one/multiple BS(s) in the system and it cooperatively serves one/multiple user(s) at the same time. By contrast, for the US-RIS, both the controller and the beneficiary is the same user. Both the beamforming design and phase-shift control are carried out at the US-RIS.

- *Operating mode and structure:* Most BSS-RISs are considered as reflective surfaces, while for US-RIS we apply the transmissive mode considering the space-limited characteristic of the user [13]. To improve the array gains, we further propose the multi-layer structure of US-RIS. Different from the single-layer structure which can only shift the phase of each incident signal, the multi-layer structure can redistribute the energy of RIS among the elements through precoding at multiple RIS layers, indicating that the amplitude of the signal can be partially controlled [14], which has structural advantages.
- *Size and element activation ratio (EAR):* For BSS-RIS-aided communications, the size of BSS-RIS is expected to be very large, which is not practical to be employed at the user side. Therefore, each layer of US-RIS should be designed to be much smaller to match the physical size. The proposed multi-layer structure can alleviate the disadvantages of the small size and increase the hardware utilization compared to a single-layer structure. To quantify, we define a metric named element activation ratio (EAR) to evaluate the proportion of RIS that mainly contributes to beamforming. In this ratio, we count an element as being "activated", if its power is higher than a threshold percentage ε of the average power. Under this definition, a RIS will have larger EAR and will form higher-gain beams if the power is distributed flatter. In Section IV-C, we provide experimental results of EAR for further demonstration.

C. System model of US-RIS-aided communications

For modeling the system, we consider the US-RIS-aided communications as shown in Fig. 3, where a multi-layer US-RIS is employed to enhance the uplink communications from the user to the BS. Suppose the user and the BS are equipped with K antennas and M antennas, respectively, and the US-RIS has L layers with N elements on each layer.

For the user working as a transmitter, denote s as the normalized transmitted symbol. The symbol s is firstly precoded by the beamforming vector $\boldsymbol{w} \in \mathbb{C}^{K\times 1}$ with power constraint $\|\boldsymbol{w}\|_2^2 \leq P_{\max}$ before transmission. For signal transmission, only the user-RIS-BS link is considered and other possible links are neglected due to unfavorable propagation conditions. Furthermore, we define the phase shift matrix of US-RIS's l-th layer as

$$\boldsymbol{\Theta}_l = \operatorname{diag}\left(\boldsymbol{\theta}_l\right) = \operatorname{diag}\left(\left[\theta_{l,1}, \cdots, \theta_{l,N}\right]^T\right), \tag{1}$$

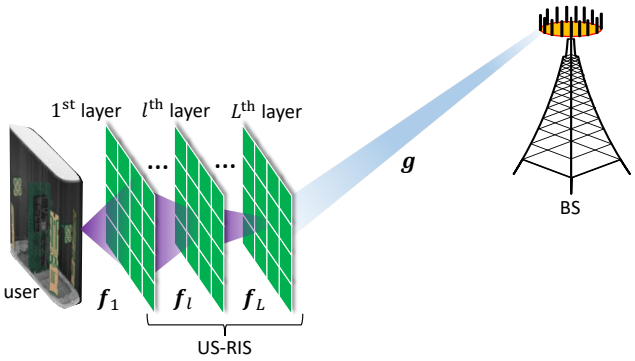

Fig. 3. System model of US-RIS-aided communications.

where $\theta_{l,n} \in \mathcal{F}$ is the phase shift of the RIS element and $\mathcal{F}$ is the feasible set of the transmission coefficient (TC). In this paper we consider a general condition that

$$\mathcal{F} = \left\{\theta \middle| \theta = e^{j\varphi}, \varphi \in [-\pi, \pi]\right\}, \tag{2}$$

which indicates that only the phase of $\theta_{l,n}$ can be controlled independently and continuously [10]. Therefore, the received signal at the BS can be represented as

$$\boldsymbol{y} = \boldsymbol{g}^H \left(\prod_{l=L}^{1} \kappa \boldsymbol{\Theta}_l \boldsymbol{f}_l\right) \boldsymbol{w} s + \boldsymbol{n}, \tag{3}$$

where κ denotes the loss factor when the electromagnetic wave penetrates each layer; $\boldsymbol{g} \in \mathbb{C}^{N\times M}$, $\boldsymbol{f}_1 \in \mathbb{C}^{N\times K}$, and $\boldsymbol{f}_l \in \mathbb{C}^{N\times N}$ denote the channels from US-RIS's L-th layer to BS, from user to US-RIS's first layer, and from US-RIS's $(l-1)$-th layer to l-th layer, for all $l \in \{2, 3, \cdots, L\}$, respectively; $\boldsymbol{n}$ denotes the additive white gaussian noise (AWGN) with power σ^2 introduced at the receiver BS. Finally, BS combines the signal received from M antennas with a combining vector $\boldsymbol{v} \in \mathbb{C}^{M\times 1}$. Thereby, the combined signal at BS can be modeled as

$$z = \boldsymbol{v}^H \boldsymbol{y} = \boldsymbol{v}^H \boldsymbol{g}^H \left(\prod_{l=L}^{1} \kappa \boldsymbol{\Theta}_l \boldsymbol{f}_l\right) \boldsymbol{w} s + \boldsymbol{v}^H \boldsymbol{n}. \tag{4}$$

III. Multi-Layer Precoding Design

Based on the developed system model, in this section, we first formulate the SNR maximization problem. Due to the non-convexity introduced by the multi-layer structure, we then propose a multi-layer precoding design to solve this problem.

A. Problem formulation

We consider to maximize the decoding SNR of the proposed US-RIS-aided communications. For the combined signal z at the BS, an equivalent noise $\boldsymbol{v}^H \boldsymbol{n}$ is introduced with variance $\left\|\boldsymbol{v}^H\right\|_2^2 \sigma^2$. Thus the decoding SNR at the BS can be represented as

$$\text{SNR} = \frac{\left|\boldsymbol{v}^H \boldsymbol{g}^H \left(\prod_{l=L}^{1} \kappa \boldsymbol{\Theta}_l \boldsymbol{f}_l\right) \boldsymbol{w}\right|^2}{\left\|\boldsymbol{v}^H\right\|_2^2 \sigma^2}. \tag{5}$$

Then, subject to the constraint of the maximum transmit power at the user and the constraint of TC at US-RIS, the SNR maximization problem can be formulated as

$$\max_{\boldsymbol{v},\boldsymbol{\Theta}_1,\cdots,\boldsymbol{\Theta}_L,\boldsymbol{w}} \text{SNR} = \frac{\left|\boldsymbol{v}^H\boldsymbol{g}^H\left(\prod_{l=L}^{1}\kappa\boldsymbol{\Theta}_l\boldsymbol{f}_l\right)\boldsymbol{w}\right|^2}{\|\boldsymbol{v}^H\|_2^2\,\sigma^2} \tag{6a}$$

$$\text{s.t.} \quad \text{C}_1: \ \|\boldsymbol{w}\|_2^2 \le P_{\max} \tag{6b}$$

$$\text{C}_2: \ |\theta_{l,n}| = 1, \ \forall l, n \tag{6c}$$

To tackle the non-convexity of the objective function, we propose the multi-layer precoding design that jointly optimizes the combining vector $\boldsymbol{v}$, US-RIS phase shift matrices $\boldsymbol{\Theta}_1,\cdots,\boldsymbol{\Theta}_L$, and the beamforming vector $\boldsymbol{w}$.

B. Overview of the proposed multi-layer precoding design

The multi-layer precoding design is summarized in **Algorithm 1**. Specifically, with the input channel matrices and parameters, we decouple the variables $\boldsymbol{v}$, $\boldsymbol{\Theta}_1,\cdots,\boldsymbol{\Theta}_L$, and $\boldsymbol{w}$ by alternately updating one variable with the other variables fixed. Until the convergence of the objective SNR is achieved, the recurrent loop ends, and the optimal solutions are obtained. Notice that SNR is changed monotonously during the updation, thus **Algorithm 1** has strict convergence.

C. Optimal beamforming, US-RIS precoding, and combining

In this subsection, we derive the closed-form expression of the optimal solutions corresponding to each variable. For ease of notation, we first denote

$$\boldsymbol{\xi}_{(p,q)} = \begin{cases} \prod_{l=p}^{q}\kappa\boldsymbol{\Theta}_l\boldsymbol{f}_l, & p\in[L], q\in[L] \\ \boldsymbol{I}_N, & p=L, q=L+1 \\ \boldsymbol{I}_K, & p=0, q=1 \end{cases}. \tag{7}$$

1) Optimal combining: For the combing vector $\boldsymbol{v}$, the optimization can be reformulated as

$$\max_{\boldsymbol{v}} \ \text{SNR} = \frac{\boldsymbol{v}^H\boldsymbol{g}^H\boldsymbol{\xi}_{(L,1)}\boldsymbol{w}\boldsymbol{w}^H\boldsymbol{\xi}_{(L,1)}^H\boldsymbol{g}\boldsymbol{v}}{\|\boldsymbol{v}^H\|_2^2\,\sigma^2} := \frac{\boldsymbol{v}^H\boldsymbol{U}\boldsymbol{v}}{\|\boldsymbol{v}^H\|_2^2\,\sigma^2}. \tag{8}$$

Algorithm 1 Multi-layer Precoding Design for US-RIS-Aided Communications

Input: Channel matrices $\boldsymbol{f}_1,\cdots,\boldsymbol{f}_L$, and $\boldsymbol{g}$; maximum transmit power $P_{\max}$; noise power σ^2; loss factor κ.

Output: Optimized combining vector $\boldsymbol{v}$; optimized US-RIS precoding matrix $\boldsymbol{\Theta}_1,\cdots,\boldsymbol{\Theta}_L$; optimized beamforming vector $\boldsymbol{w}$; maximized SNR.

1: Initialize $\boldsymbol{v}$, $\boldsymbol{\Theta}_1,\cdots,\boldsymbol{\Theta}_L$, and $\boldsymbol{w}$;
2: **while** no convergence of SNR **do**
3: Update $\boldsymbol{v}^{\text{opt}}$ by (9);
4: Update $\boldsymbol{\Theta}_1^{\text{opt}},\cdots,\boldsymbol{\Theta}_L^{\text{opt}}$ in term by (12);
5: Update $\boldsymbol{w}^{\text{opt}}$ by (15);
6: Update SNR by (5);
7: **end while**
8: **return** $\boldsymbol{v}$, $\boldsymbol{\Theta}_1,\cdots,\boldsymbol{\Theta}_L$, $\boldsymbol{w}$, and SNR.

where $\boldsymbol{U} = \boldsymbol{g}^H\boldsymbol{\xi}_{(L,1)}\boldsymbol{w}\boldsymbol{w}^H\boldsymbol{\xi}_{(L,1)}^H\boldsymbol{g}$ is a positive semidefinite matrix. Based on matrix analysis, the maximum SNR is obtained when $\boldsymbol{v}$ is the eigenvector of $\boldsymbol{U}$ corresponding to its largest eigenvalue, i.e.,

$$\boldsymbol{v}^{\text{opt}} = \psi_{\max}\left(\boldsymbol{g}^H\boldsymbol{\xi}_{(L,1)}\boldsymbol{w}\boldsymbol{w}^H\boldsymbol{\xi}_{(L,1)}^H\boldsymbol{g}\right). \tag{9}$$

2) Optimal US-RIS precoding: For the precoding matrix $\boldsymbol{\Theta}_l, l\in[L]$, noticing that $\boldsymbol{\Theta}_l = \text{diag}(\boldsymbol{\theta}_l)$ is a diagonal matrix and $\boldsymbol{f}_l\boldsymbol{\xi}_{(l-1,1)}\boldsymbol{w}$ is a column vector, we have

$$\boldsymbol{\xi}_{(l,1)}\boldsymbol{w} = \text{diag}(\boldsymbol{f}_l\boldsymbol{\xi}_{(l-1,1)}\boldsymbol{w})\boldsymbol{\theta}_l. \tag{10}$$

With the transformation (10), SNR can be rewritten as

$$\begin{aligned}\text{SNR} &= \frac{\left|\boldsymbol{v}^H\boldsymbol{g}^H\boldsymbol{\xi}_{(L,1)}\boldsymbol{w}\right|^2}{\|\boldsymbol{v}^H\|_2^2\,\sigma^2} \\ &= \frac{\left|\boldsymbol{v}^H\boldsymbol{g}^H\boldsymbol{\xi}_{(L,l+1)}\boldsymbol{\xi}_{(l,1)}\boldsymbol{w}\right|^2}{\|\boldsymbol{v}^H\|_2^2\,\sigma^2} \\ &= \frac{\left|\boldsymbol{v}^H\boldsymbol{g}^H\boldsymbol{\xi}_{(L,l+1)}\text{diag}(\boldsymbol{f}_l\boldsymbol{\xi}_{(l-1,1)}\boldsymbol{w})\boldsymbol{\theta}_l\right|^2}{\|\boldsymbol{v}^H\|_2^2\,\sigma^2}.\end{aligned} \tag{11}$$

Considering the constraint (6c), the optimal value of $\boldsymbol{\theta}_l$ is obtained when all components of $\boldsymbol{\theta}_l$ have the complementary phase angle as the vector multiplied on its left, i.e.,

$$\boldsymbol{\theta}_l^{\text{opt}} = \exp\left(j\arg\left(\text{diag}\left(\boldsymbol{f}_l\boldsymbol{\xi}_{(l-1,1)}\boldsymbol{w}\right)^H\boldsymbol{\xi}_{(L,l+1)}^H\boldsymbol{g}\boldsymbol{v}\right)\right). \tag{12}$$

3) Optimal beamforming: At last, for the beamforming vector $\boldsymbol{w}$, we first consider the optimization for the normalized vector $\langle\boldsymbol{w}\rangle$, i.e.,

$$\begin{aligned}\max_{\langle\boldsymbol{w}\rangle} \ &\frac{\left|\boldsymbol{v}^H\boldsymbol{g}^H\boldsymbol{\xi}_{(L,1)}\langle\boldsymbol{w}\rangle\right|^2}{\|\boldsymbol{v}^H\|_2^2\,\sigma^2} = \frac{\text{SNR}}{\|\boldsymbol{w}\|_2^2} \\ \text{s.t.} \ &\|\langle\boldsymbol{w}\rangle\|_2 = 1\end{aligned} \tag{13}$$

We obtain the optimized $\langle\boldsymbol{w}\rangle$ as

$$\langle\boldsymbol{w}\rangle^{\text{opt}} = \left\langle\boldsymbol{\xi}_{(L,1)}^H\boldsymbol{g}\boldsymbol{v}\right\rangle. \tag{14}$$

Noticing the constraint (6b), the optimized $\boldsymbol{w}$ for (6) and the optimized $\langle\boldsymbol{w}\rangle$ for (13) has the relation

$$\boldsymbol{w}^{\text{opt}} = \sqrt{P_{\max}}\,\langle\boldsymbol{w}\rangle^{\text{opt}} = \sqrt{P_{\max}}\left\langle\boldsymbol{\xi}_{(L,1)}^H\boldsymbol{g}\boldsymbol{v}\right\rangle. \tag{15}$$

IV. Simulation Results

In this section, we provide simulation results to demonstrate the superior performance of the proposed concept of US-RIS and the corresponding multi-layer precoding design.

A. Simulation setup

For simplicity but without loss of generality, we consider a scenario with the topology as shown in Fig. 4, where different types of RISs are employed to assist communications from the user to the BS. We assume that both the user and the BS are equipped with uniform linear array (ULA) with 2 and 8 antennas, respectively. A multi-layer US-RIS, with 2 layers and 8×12 elements on each layer, is employed as shown in Fig. 4 (a). For comparison, we consider two more benchmarks

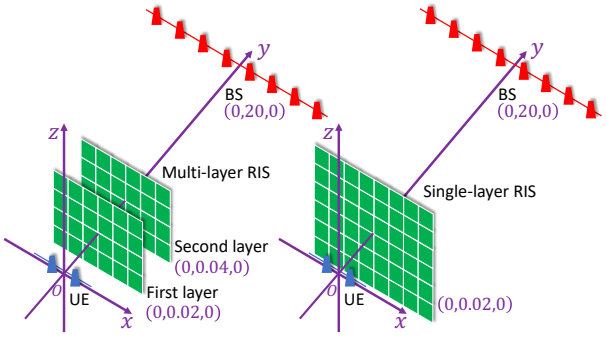

Fig. 4. The simulation scenario where different types of RISs are deployed to assist communications. (a) Multi-layer US-RIS-aided communications. (b) Single-layer US/BSS-RIS-aided communications.

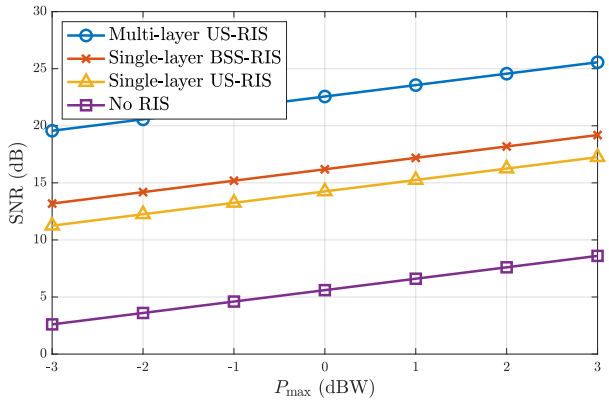

Fig. 5. Decoding SNR against maximum transmit power $P_{\max}$.

that, a single-layer US-RIS (or a single-layer reflective BSS-RIS) with 12×16 elements is deployed at the same position as the multi-layer US-RIS's first layer shown in Fig. 4 (b). We assume that the user, multi-layer US-RIS's first layer (located at the same position as single-layer US/BSS-RIS), multi-layer US-RIS's second layer, and BS are located with its center at $(0\,\mathrm{m}, 0\,\mathrm{m}, 0\,\mathrm{m})$, $(0\,\mathrm{m}, 0.02\,\mathrm{m}, 0\,\mathrm{m})$, $(0\,\mathrm{m}, 0.04\,\mathrm{m}, 0\,\mathrm{m})$, and $(0\,\mathrm{m}, 20\,\mathrm{m}, 0\,\mathrm{m})$, respectively. The frequency of the transmitted signal is $f = 2.5\,\mathrm{GHz}$. The noise power is $\sigma^2 = 1 \times 10^{-6}$. The loss factor is $\kappa = 0.8$.

Finally, for the proposed multi-layer precoding design, we assume that the channel state information (CSI) is perfectly known [9], which can be obtained through existing channel estimation methods [15]. Specifically, in US-RIS-aided communications, the channel from the user to RIS and the inter-layer channels can be estimated beforehand thanks to stability produced by enclosing materials.

B. Performance of received signal with different usages of RIS

The performance of the proposed US-RIS-aided communications is evaluated in this subsection. As shown in Fig. 5, we consider the decoding SNR against the maximum transmit power $P_{\max}$ with different usages of RIS. We also consider a *"No RIS"* benchmark for comparison, where RIS shown in Fig. 4 is removed.

From Fig. 5 we can notice that, SNR and maximum transmit power $P_{\max}$ has almost a linear relationship which can also be observed from the parameter updates. Therefore, we can just compare different cases with the maximum transmit power $P_{\max}$ fixed. First, it can be observed that the transmission without RIS has the lowest SNR, which indicates that all usages of RIS can substantially enhance the communications. Another observation is that the single-layer US-RIS-aided communications has a $1.94\,\mathrm{dB}$ loss compared to the single-layer BSS-RIS-aided communications, which is caused by the existence of loss factor. Moreover, the multi-layer US-RIS-aided communications has a $6.37\,\mathrm{dB}$ increment compared to the single-layer BSS-RIS-aided communications with the same number of total elements. This significant SNR improvement further demonstrates the structural superiority compared to conventional single-layer structure.

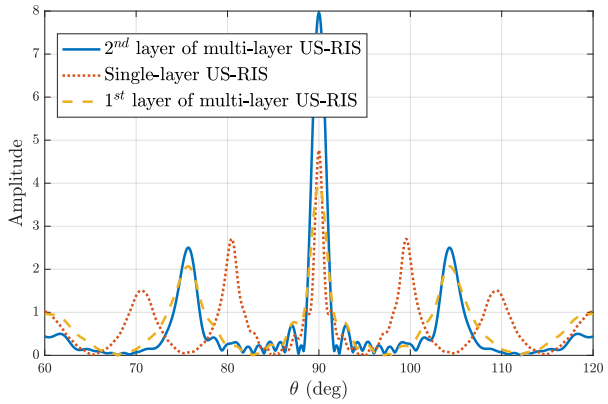

Fig. 6. Radiation patterns of different RISs.

To unravel the nature of the multi-layer structure, we present the radiation patterns of different RISs in Fig. 6. In the radiation pattern, we evaluate the quality of a beam by its mainlobe and sidelobes. The beam with a higher mainlobe and lower sidelobes is preferred. From Fig. 6, we can observe that the transmitted beam of the first layer of multi-layer US-RIS has a higher mainlobe compared to the transmitted beam of single-layer US-RIS, which is caused by the inferior in the number of elements. However, after penetrating the second layer, sidelobes are considerably weakened while a higher main lobe forms, compared to both the first layer and the single-layer US-RIS. The above results coincide with the analysis on receiving SNR well.

C. Analysis on RIS's element utilization ratio

To further reveal the function of the multi-layer structure, in this subsection we discuss the power distribution of multi-layer US-RIS and single-layer US-RIS, as shown in Fig. 7. The reason why single-layer US-RIS performs worse is that the marginal RIS elements have not been sufficiently excavated.

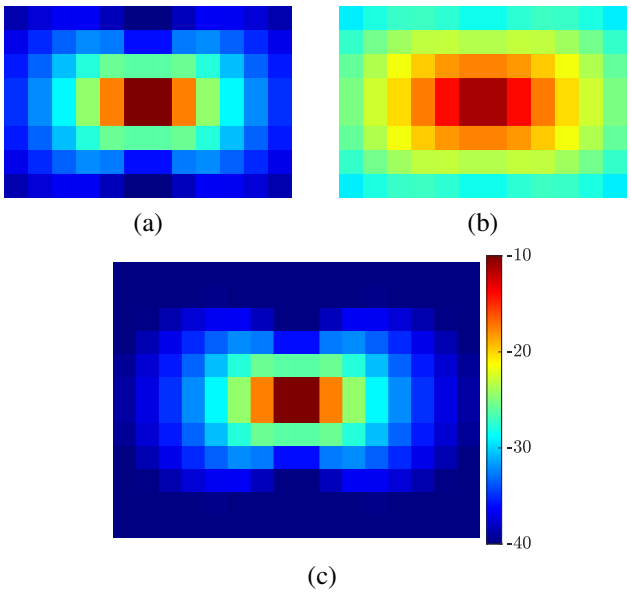

Fig. 7. Power distribution of multi-layer and single-layer US-RIS (colorbar on the right is unified for 3 subfigures, unit: dBW), implying different EARs of different RISs. Threshold percentage is set to $\varepsilon = 1/6$. (a) The first layer of multi-layer US-RIS with EAR 29.2%. (b) The second layer of multi-layer US-RIS with EAR 87.5%. (c) Single-layer US-RIS with EAR 22.9%.

It can be directly observed from Fig. 7 (a) and (c) that in first layer of multi-layer US-RIS and single-layer US-RIS, central elements occupy most of the power while elements in the outer loop have little contribution. However, in the second layer of US-RIS as shown in Fig. 7 (b), with the help of the phase shift control on first layer, the power distribution is transformed to a flatter pattern. Although the power of central elements declines, the elements along the edges become more influential.

To quantify this phenomenon, we apply the metric EAR defined in Section II-B to analyze the hardware utilization of RIS. The EARs of different RISs with threshold percentage $\varepsilon = 1/6$ are given in Fig. 7. The first layer of the multi-layer US-RIS has an EAR of 29.2%, which is higher than that of the single-layer US-RIS having an EAR of 22.9%, because the first layer of the multi-layer US-RIS has fewer elements. Furthermore, as a benefit of the multi-layer structure, the EAR of the second layer of the US-RIS is 87.5%, and the overall EAR of the multi-layer US-RIS is 58.3%, which is twice higher than that of the single-layer US-RIS. The obvious improvement in EAR also demonstrates the ascendancy of the proposed architecture with multi-layer structure.

V. Conclusions

In this paper, we have proposed the concept of US-RIS as a solution to deploying a large-scale array at the user side. Different from existing usages of RIS which can all be categorized as BSS-RISs, US-RIS is the first usage of RIS as a hardware technique at the user side. We have also proposed a novel user architecture equipped with multi-layer US-RIS. Moreover, we have formulated the SNR maximization problem in the US-RIS-aided communications. To solve the problem, we have proposed a multi-layer precoding design that alternately solves the optimal solutions for each variable. Simulation results demonstrate that, compared with the existing BSS-RISs, the proposed multi-layer US-RIS as a realization of the large-scale array at the user side appears a higher performance in enhancing wireless transmissions.

Acknowledgment

This work was supported in part by the National Key Research and Development Program of China (Grant No. 2020YFB1807201), in part by the National Natural Science Foundation of China (Grant No. 62031019), and in part by the European Commission through the H2020-MSCA-ITN META WIRELESS Research Project (Grant No. 956256).

References

[1] S. Parkvall, E. Dahlman, A. Furuskar, and M. Frenne, "NR: The new 5G radio access technology," *IEEE Commun. Standards Mag.*, vol. 1, no. 4, pp. 24–30, Apr. 2017.

[2] T. L. Marzetta, "Noncooperative cellular wireless with unlimited numbers of base station antennas," *IEEE Trans. Wireless Commun.*, vol. 9, no. 11, pp. 3590–3600, Nov. 2010.

[3] E. Basar, M. Di Renzo, J. De Rosny, M. Debbah, M.-S. Alouini, and R. Zhang, "Wireless communications through reconfigurable intelligent surfaces," *IEEE Access*, vol. 7, pp. 116 753–116 773, Aug. 2019.

[4] L. Dai, B. Wang, M. Wang, X. Yang, J. Tan, S. Bi, S. Xu, F. Yang, Z. Chen, M. Di Renzo, C.-B. Chae, and L. Hanzo, "Reconfigurable intelligent surface-based wireless communications: Antenna design, prototyping, and experimental results," *IEEE Access*, vol. 8, pp. 45 913–45 923, Mar. 2020.

[5] C. Pan, H. Ren, K. Wang, J. F. Kolb, M. Elkashlan, M. Chen, M. Di Renzo, Y. Hao, J. Wang, A. L. Swindlehurst, X. You, and L. Hanzo, "Reconfigurable intelligent surfaces for 6G systems: Principles, applications, and research directions," *IEEE Commun. Mag.*, vol. 59, no. 6, pp. 14–20, Jun. 2021.

[6] C. Huang, A. Zappone, G. C. Alexandropoulos, M. Debbah, and C. Yuen, "Reconfigurable intelligent surfaces for energy efficiency in wireless communication," *IEEE Trans. Wireless Commun.*, vol. 18, no. 8, pp. 4157–4170, Aug. 2019.

[7] Z. Zhang, L. Dai, X. Chen, C. Liu, F. Yang, R. Schober, and H. V. Poor, "Active RIS vs. passive RIS: Which will prevail in 6G?" *arXiv preprint arXiv:2103.15154*, Mar. 2021.

[8] K. Liu and Z. Zhang, "On the energy-efficiency fairness of reconfigurable intelligent surface-aided cell-free network," in *Proc. 2021 IEEE 93rd Veh. Technol. Conf. (IEEE VTC'21 Spring)*, 2021, pp. 1–6.

[9] Z. Zhang and L. Dai, "A joint precoding framework for wideband reconfigurable intelligent surface-aided cell-free network," *IEEE Trans. Signal Process.*, vol. 69, pp. 4085–4101, Aug. 2021.

[10] Q. Wu and R. Zhang, "Intelligent reflecting surface enhanced wireless network via joint active and passive beamforming," *IEEE Trans. Wireless Commun.*, vol. 18, no. 11, pp. 5394–5409, Aug. 2019.

[11] Y. Lu and L. Dai, "Reconfigurable intelligent surface based hybrid precoding for THz communications," *arXiv preprint arXiv:2012.06261*, Dec. 2020.

[12] Z. Yang, W. Xu, C. Huang, J. Shi, and M. Shikh-Bahaei, "Beamforming design for multiuser transmission through reconfigurable intelligent surface," *IEEE Trans. Commun.*, vol. 69, no. 1, pp. 589–601, Jan. 2021.

[13] S. Zeng, H. Zhang, B. Di, Y. Tan, Z. Han, H. V. Poor, and L. Song, "Reconfigurable intelligent surfaces in 6G: Reflective, transmissive, or both?" *IEEE Commun. Lett.*, vol. 25, no. 6, pp. 2063–2067, Jun. 2021.

[14] J. Wang, W. Tang, Y. Han, S. Jin, X. Li, C.-K. Wen, Q. Cheng, and T. J. Cui, "Interplay between RIS and AI in wireless communications: Fundamentals, architectures, applications, and open research problems," *arXiv preprint arXiv:2101.00250*, Jan. 2021.

[15] C. Hu, L. Dai, S. Han, and X. Wang, "Two-timescale channel estimation for reconfigurable intelligent surface aided wireless communications," *IEEE Trans. Commun.*, Apr. 2021.